

Tin Coatings Electrodeposited from Sulfonic Acid-Based Electrolytes: Tribological Behavior

L.N. Bengoa, W.R. Tuckart, N. Zabala, G. Prieto, and W.A. Egli

(Submitted November 7, 2014; in revised form March 25, 2015; published online April 9, 2015)

A high efficiency methane sulfonic acid electrolyte used for tin electrodeposition was studied, and the properties of the resulting deposits were compared to those of tin coatings obtained from an industrial phenol sulfonic acid electrolyte. Cyclic voltammetry was used to study the effect of organic additives on the reduction process to define the composition of the electrolytic bath. Thick tin electrodeposits were obtained on rotating cylinder steel electrodes, and their surface morphology, preferred crystal orientation, surface roughness, micro hardness, and tribological behavior were measured. Smooth, adherent, and bright tin coatings were obtained from the methane sulfonic acid electrolyte, which differed in morphology and texture from tin electrodeposited from the industrial bath. Influence of organic additives on preferred crystal orientation of the coatings was found to be stronger than changing the supporting sulfonic acid type. Tribological tests showed that the two types of deposits have a similar coefficient of friction. However, tin coatings obtained from methane sulfonic electrolytes presented a lower wear resistance and underwent galling at lower loads.

Keywords coatings, methane sulfonic acid, phenol sulfonic acid, tin, tribology, wear resistance

1. Introduction

Electrodeposition of metals, also known as electroplating, is a commonly used technique that allows modifying the surface properties of a metallic substrate. Throughout the years, several metallic coatings have been developed to obtain products with different characteristics. A survey of all the metals that can be electrodeposited was made by Winand (Ref 1) who also classified them into three groups according to their electrochemical behavior. Among these, tin deposits provide numerous beneficial properties such as excellent solderability, ductility, softness, and corrosion or tarnish resistance (Ref 2). For this reason, they have been found to be suitable for many applications, mainly in the food and the electronic industries. Tin also has a good lubricity (Ref 3) which is a necessary requirement for the production of drawn and wall-ironed cans, and aerosol valves and domes (Ref 4), used mainly as beverage, food, and general uses containers. In these processes, the tin coatings are severely deformed in short times and in some cases they are completely destroyed leaving the steel substrate partially exposed.

Electrodeposited tin coatings are industrially produced from a number of different electrolytes. One of these is the phenol

sulfonic acid (PSA) chemistry, mostly used during the last decades in the steel plating industry due to its ability to operate at high current densities (Ref 3). Although this bath has been used for a long time, it has some important drawbacks. First, there is a continuous loss of tin caused by the spontaneous oxidation of stannous to stannic tin (Ref 5-7). The latter not only leads to an increase in the operation costs but also produces a sludge which can affect both the product quality and the production throughput (Ref 8). In addition, due to the presence of the toxic phenol group, electrolyte handling and its waste disposal process is rather complex.

To overcome the inherent difficulties of the PSA, different alternative chemistries have been studied (Ref 3, 9-12). Among these, a methane sulfonic acid (MSA) based bath has gained acceptance over the years as an alternative for PSA in the continuous steel strip plating process (Ref 13, 14). The MSA-based electrolytes have higher conductivity, which lowers the concentration of tin needed to achieve good quality coatings and reduces the operation costs. In contrast to PSA, MSA does not act as an antioxidant limiting stannous tin oxidation, and for that reason 1 g/L hydroquinone (HQ) is usually added, which fulfills that function. A further advantage of this chemistry is that MSA effluents are easy to treat (Ref 15).

Many MSA + HQ-based tin-plating baths containing a variety of organic additives have been formulated and studied (Ref 16-22). On the other hand, some authors have focused their efforts on evaluating the properties of the resulting tin deposits (Ref 23, 24). Nonetheless, even though there are plenty of articles dealing with tin electrodeposition from either PSA or MSA baths, none of these works investigated both chemistries simultaneously. Furthermore, no direct comparison of the mechanical and tribological properties of tin coatings obtained from PSA and MSA electrolytes with similar compositions has been made yet, to our knowledge. As mentioned earlier, these properties play a major role in some particular applications of tin coatings and, therefore, the lack of such information is a relevant issue.

In the present work, tin coatings deposited from two similar electrolytes with PSA and MSA as supporting acids are

L.N. Bengoa, Centre for Paints and Coatings Development, CICBA-CONICET, Av. 52 e/121 y 122, La Plata, Argentina and School of Engineering, Universidad Nacional de La Plata, Av. 1 y 47, La Plata, Argentina; W.R. Tuckart, N. Nabala, and G. Prieto, Tribology Group, Engineering Department, Universidad Nacional del Sur, CONICET, Av. Alem 1253, 1° Piso, 8000 Bahía Blanca, Buenos Aires, Argentina; and W. A. Egli, Centre for Paints and Coatings Development - CICBA-CONICET, Av. 52e/121y121, La Plata, Argentina. Contact e-mails: leandrobengoa@gmail.com and anelpire4@cidepint.gov.ar.

characterized, and their tribological properties are compared. Special attention is paid to the effect of the acids and the organic additives on surface morphology and crystal orientation.

2. Materials and Methods

2.1 Cyclic Voltammetry (CV)

To evaluate the general electrochemical behavior and the effect of the addition of different organic additives to the electrolytes, CV was carried out. The latter was performed using an EG&G Princeton Applied Research Potentiostat/Galvanostat (Mod. 273A) coupled to a personal computer controlled by CorrWare2[®] software. A 0.041 cm² Pt rotating disk electrode (RDE) was used as working electrode and its electrochemical potential was measured using a saturated calomel electrode (SCE) with a Lugging capillary. All the potential values in this paper are expressed on the SCE scale. A Pt wire (1.6 cm²) was used as counter electrode. All the voltammograms were recorded at a scan rate of 20 mV/s at a rotating speed of 500 rpm. Using data fitting tools, the CV stripping efficiency was calculated as the ratio of the charge integrated under the anodic sweep (Q_{an}) to the charge integrated under the cathodic sweep (Q_{cat}) during one voltammetric cycle.

2.2 Electrodeposition Experiments

For tin coating deposition, two different solutions were prepared. A commercial Ferrostan bath (PSA-based) was chosen for being widely used in tinning industry. For comparison, a different electrolyte was formulated by changing the PSA for MSA. Diphone 6 (D6), a commercial brightener for tin electrodeposition, was used for both electrolytes. To improve the coating surface morphology, polyethylene glycol (MW 600) was also added to MSA electrolyte. The composition of both solutions, reported in Table 1, was defined according to values found in the literature (Ref 8, 16, 18, 21, 25). All the chemicals used in this work were reagent grade (Table 2).

Tin coatings were electrodeposited on low carbon steel rotating cylinder electrodes (RCE), 5 cm long and 0.8 cm diameter, using a tin cylinder as anode to attain a uniform current distribution (Ref 26, 27). A detailed description of the

experimental set up has been given in a previous work (Ref 28). Prior to electrodeposition experiments, the substrates were electrochemically degreased, in a 30 g/L NaOH solution at a cathodic current density (CD) of 64 A/dm² at 30 °C and then pickled in 10% sulphuric acid at 70 °C. Immediately afterward, these were rinsed and immersed in the electroplating bath to prevent oxidation. All the coatings in this work were obtained galvanostatically at a cathode rotation speed of 500 rpm (42 cm/s peripheral velocity). To optimize plating performance, the electrolyte temperature was adjusted to commonly found values in the literature (Ref 3, 9, 15, 19) (Table 1).

2.3 Deposits Characterization and Evaluation

The resulting coatings were characterized using scanning electron microscopy (SEM) and x-ray diffraction (XRD). SEM micrographs were taken with a Quanta200 FEI microscope (Tungsten filament source) to analyze the surface morphology of the deposits. XRD patterns of the coatings were determined with a Phillips X'Pert diffractometer with a CuK α = 1.5405 Å. The detector scan mode with a step size of 0.05° and a sampling time of 3 s was used (scan rate 0.0167°/s). The preferred crystal orientation of the deposits was estimated by means of the relative texture coefficient $RTC_{(hkl)}$. The latter was calculated using Eq 1 (Ref 29, 30):

$$RTC_{(hkl)} = \frac{I_{hkl}/I_{hkl}^0}{\sum I_{hkl}/I_{hkl}^0} \times 100 \quad (\text{Eq 1})$$

where I_{hkl} and I_{hkl}^0 are the diffraction intensities of the crystal plane (hkl) in the sample and a standard Sn powder sample with random orientation (Ref 31), respectively.

Surface roughness was evaluated by means of a profilometer Hommel-Etamic T500 and Etamic software in accordance with ISO 3274:1996. In addition, hardness measurements were made with a Vickers micro hardness measuring device. The reported values for each sample are the results of at least ten measurements.

Samples of the coatings were embedded in an epoxy resin and mechanically ground with 800 to 2500 grade silicon paper. Finally, the samples were polished with 6 and 1 μm diamond paste, and Faradaic efficiency (FE) was quantified through coating thickness measurements from SEM micrographs of the cross sections assuming that coating density is the same as pure tin (7.31 kg/dm³).

Table 1 PSA-based and MSA-based baths compositions

Electrolyte	Sn ⁺² , g/L	MSA, mL/L	PSA, H ₂ SO ₄ g/L	D6, g/L	HQ, g/L	Temp., °C
PSA	30	...	20	8	...	30
MSA	15	21	1	40

Table 2 Chemicals used

Chemical component	Nomenclature	Function of bath components
SnSO ₄ Sigma-Aldrich 95%	...	Provides Sn ²⁺ for tin deposition
Methane sulfonic acid anhydrous (Aldrich)	MSA	Provides acidity and ionic conductivity
Phenol sulfonic acid (acidity 234.53 g H ₂ SO ₄ /l)	PSA	Provides acidity, ionic conductivity and Sn ²⁺ stability
Diphone 6	D6	Commercial brightener for Sn. Aromatic sulfonated derivative.
Hydroquinone Anedra 99%	HQ	Slows down oxidation of Sn ²⁺ to Sn ⁴⁺
Polyethylene glycol Sigma-Aldrich (MW 600)	PEG 600	Additive

Tribological behavior of coatings was evaluated by means of dry sliding wear tests. These were performed employing a homemade ball on ring system. The samples were rotated at a constant speed of 12 rpm (0.3 m/s) against a 6.35 mm diameter SAE 52100 steel ball (the counter-body). Contact loads of 5 and 10 N (normal force) were used and the total sliding distance was fixed at 170 cm. All the sliding wear experiments were run in a controlled environment: (25 ± 1) °C and 50-55% relative humidity. In order to estimate the wear rate, the width of wear track from optical microscopy (OM) images was measured. The damaged coating volume was calculated assuming that the counter-body remained unchanged. The reported results are an average of at least two runs. During the tests, the coefficient of friction (CoF) was recorded and the value was defined according to the standard ASTM G 115- 04.

3. Results and Discussion

3.1 Tin Electrodeposition

Tin deposits obtained from the PSA electrolyte at $CD = 2.5 \text{ A/dm}^2$ presented a surface morphology with a grain size around $15 \mu\text{m}$, as seen in Fig. 1. As usual, they have low glossiness which may be a consequence of the absence of a preferred crystal orientation (Ref 23, 24) observed in the XRD pattern of these samples (Fig. 2). This is also verified by the existence of five crystallographic planes showing a RTC value higher than 10% (Table 3). Under these experimental conditions, the FE was 100%, calculated as described in the experimental section.

Figure 3 shows a CV recorded in this electrolyte. A cathodic CD is registered from $E \approx -0.49 \text{ V}$ to $E \approx -0.75 \text{ V}$, which grows continuously due to Sn deposition from Sn^{+2} reduction and simultaneous hydrogen evolution. A small peak is observed at $E \approx -0.58 \text{ V}$, indicative of a nucleation and growth mechanism controlled by diffusion (Ref 32). In addition, the typical cross-over ascribed to a 3D nucleation mechanism is present (Ref 33, 34). A similar behavior has been observed during tin electrodeposition from sulfate solutions (Ref 35, 36). On the anodic branch of the CV ($E > -0.45 \text{ V}$) a single peak, corresponding to tin dissolution, appears at $E \approx -0.20 \text{ V}$. The CV stripping efficiency ($Q_{\text{an}}/Q_{\text{cat}}$) was estimated to be 92%, which confirms the existence of a secondary cathodic process (mainly H_2 evolution).

A tin coating from the MSA electrolyte without additives was obtained at $CD = 1 \text{ A/dm}^2$. The resulting deposit was dendritic and did not cover the substrate completely. This behavior can be explained on the basis of dendritic growth theory. According to Popov et al. (Ref 37, 38), dendrites can grow even at small current densities when the reaction has a large exchange current density. This is the case of tin reduction kinetics in MSA electrolytes, which are very facile in the absence of additives (Ref 17). The voltammetric response of tin electrodeposition in this electrolyte is shown in Fig. 4 (dashed line), which presents similar features to those observed in PSA electrolytes. No significant differences can be appreciated in tin discharge ($E = -0.44 \text{ V}$) and dissolution peak ($E = -0.24 \text{ V}$) potentials, although no reduction peak is observed. It is worth noting that the latter may appear if more cathodic potentials are reached on the cathodic sweep of the CV, as has been reported before (Ref 36). Despite this, the stripping efficiency for the

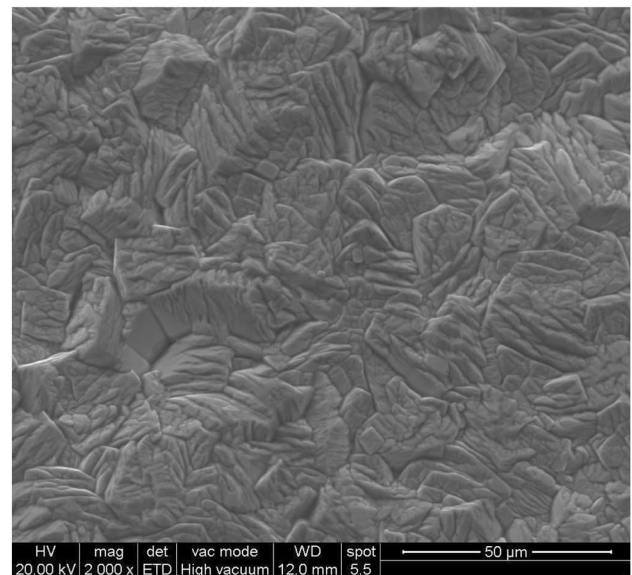


Fig. 1 SEM image for Sn coating (PSA) $\times 2000$

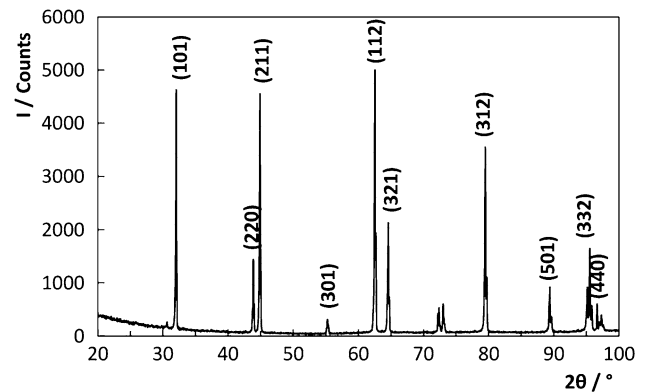


Fig. 2 XRD pattern of Sn deposit obtained from PSA

Table 3 Relative texture coefficients of tin deposits obtained from different electrolytes

Plane (<i>hkl</i>)	RTC (%)		
	PSA + D6	MSA + D6	MSA + D6 + PEG
200	0.0	0.6	0.0
101	1.9	2.6	0.0
220	1.5	0.7	9.8
211	3.0	1.8	0.1
301	1.1	3.5	0.1
112	11.6	14.1	0.0
400	0.1	1.6	0.3
321	2.8	2.6	2.9
420	2.4	1.9	3.7
411	1.3	1.6	0.7
312	11.5	7.4	0.1
501	5.5	1.5	4.9
103	16.1	35.1	1.0
332	21.8	18.4	0.9
440	15.3	0.9	68.6
521	4.1	5.6	7.1

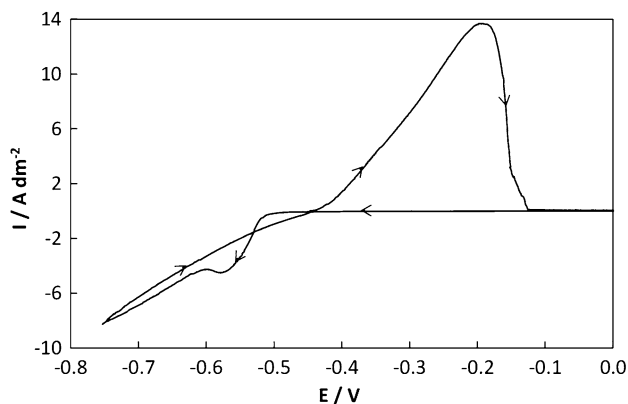


Fig. 3 CV for PSA electrolyte, recorded at 20 mV/s and 500 rpm

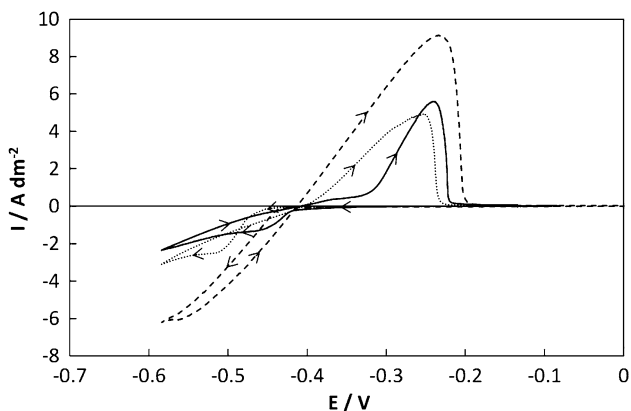


Fig. 4 CV of MSA electrolyte (dashed line) without additives, (solid line) with D6 and (dotted line) with D6 + PEG, recorded at 20 mV/s and 500 rpm

MSA electrolyte was found to be almost equal (95%) to the one for the PSA bath.

In order to improve coatings quality, the addition of organic additives was required. It was found in literature (Ref 17, 39, 40) that aromatic organic compounds affect both the polarization curves and the deposit morphology. D6, a bisphenol-sulfonated derivative, was added to MSA electrolyte and CVs were recorded. Comparison of these curves for MSA electrolyte with and without D6 (Fig. 4, dashed and full lines) shows that this compound strongly inhibits the deposition process, reducing tin reduction current (Ref 17). This is also verified by a 43% reduction in the anodic peak area. An interesting feature of this voltammogram is that, when D6 is present, a small cathodic current is registered as from $E = -0.34$ V, which increases slowly up to $E = -0.42$ V. At that point, a change in the curve's slope is clearly detected. A similar behavior is observed during the reverse scan, in which a small steadily increasing anodic current is registered in the potential region -0.42 V $< E < -0.34$ V. It is possible that the presence of D6 promotes the under potential deposition of tin creating a phase which redissolves in the same potential window, generating the aforementioned electrochemical response. On the other hand, it may be the result of an adsorption process in which the additive is involved. However, to fully understand the phenomena undergoing in the D6-containing MSA electrolyte, further

studies are needed which are beyond the scope of this work. The CV also shows that crossing-over does not occur in contrast to the previous electrolytes studied. The latter suggests that a loose non-adherent phase, probably powdery, forms instead of a tin coating (Ref 41). Accordingly, the addition of D6 reduces the stripping efficiency to 86%.

Taking this result into account and setting standard deposition parameters for tin plating, a homogeneous, dull, and rough deposit was obtained from the MSA bath containing 8 g/L D6 at 40°C and applying 1 A/dm² during 80 min. SEM micrographs of this coating (Fig. 5a) showed a morphology consisting in 3 to 4 μ m rounded crystals growing over ≈ 15 μ m flat square-shaped structures.

Although the bath was capable of producing a compact coating covering the whole surface of the electrode, the appearance of this deposit was considerably different from that of industrial tin coatings. Martyak et al. (Ref 17) found that addition of PEG to MSA electrolytes suppressed hydrogen evolution and produced just slight modifications of deposit morphology. For this reason and to reduce the surface roughness, an addition of 2.5 g/L of PEG 600 was made. The CV of a MSA electrolyte containing D6 and PEG 600 is shown in Fig. 4 (dotted line). It can be seen that in the presence of both additives, tin reduction does not occur until the potential reaches a value of $E = -0.46$ V. Considering that D6 alone inhibits the reduction process but does not appreciably polarize it, this further polarization of tin deposition onset may be the result of a synergetic effect between D6 and PEG 600 (Ref 40, 41). In contrast, the cathodic current is higher than for D6 alone as it also is the amount of tin deposited (verified by the charges involved in the dissolution peaks). Furthermore, the stripping efficiency is also higher than that estimated for an electrolyte without PEG 600.

With the addition of PEG to the previous solution, the resulting deposit was smooth and bright despite the same operating conditions. Figure 5(b) shows the grain morphology of this coating with a larger grain size (~ 25 μ m), characteristic of satin bright tin (Ref 3). Comparison of Fig. 5(a) and (b) confirms the influence of PEG on tin morphology in MSA electrolytes. The XRD patterns of these samples illustrate the effect of both supporting electrolyte and additives on deposit's microstructure. Figure 6(a) shows the results corresponding to a coating obtained from a MSA bath containing D6. Comparing the latter with Fig. 2 (coating deposited from a PSA + D6 bath), it is clear that MSA reduces the intensities of several planes, especially (220), (211), (440), and (321). However, the RTC analysis indicates that the preferred crystal orientation is only modified to a slight degree, as the planes with the highest texture coefficient are the same in both cases, except for plane (440). When PEG 600 is added to the solution, the number of peaks detected decreases considerably. There is no signal whatsoever corresponding to the planes (200) and (101), which present the higher intensities in the standard sample. Furthermore, this additive strongly promotes the preferential growth of parallel planes (440) and (220), which could account for the bright appearance of the surface when this additive is present (Ref 23, 24). This effect is further verified by the RTC values of the aforementioned planes, which are the only remarkable ones. Such strong influence of PEG on the microstructure of electrodeposited tin has been reported before (Ref 42). In contrast with the previous deposit, coating produced from a bath containing PEG 600 was comparable to industrial tin

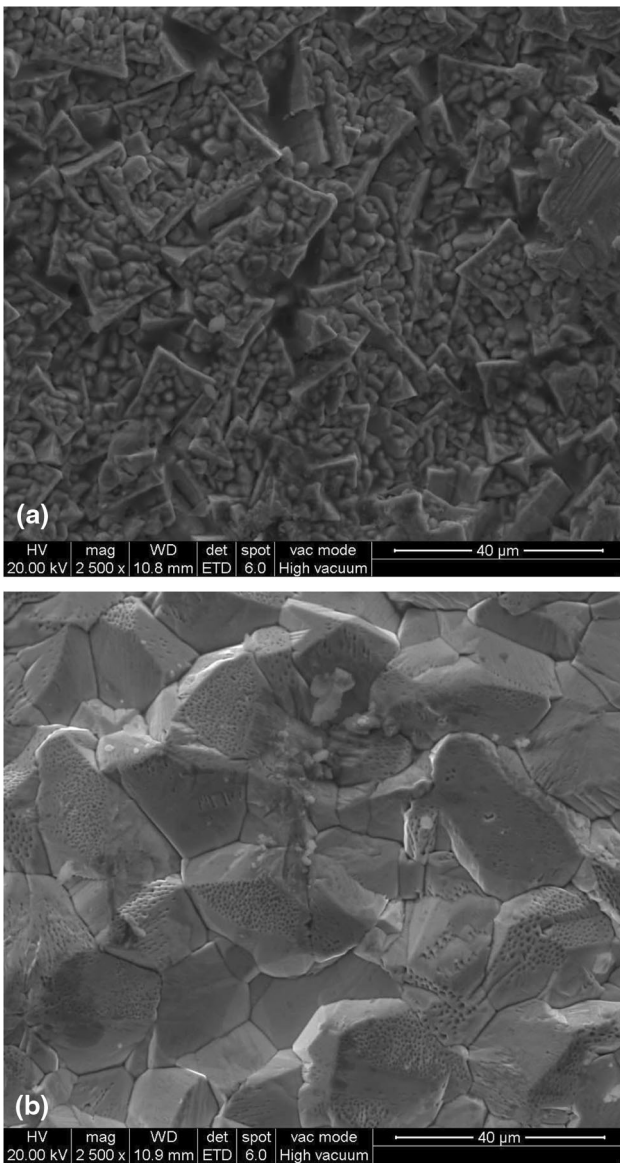


Fig. 5 SEM images of Sn coatings: (a) MSA + D6 and (b) MSA + D6 + PEG ($\times 2500$)

coatings. The estimated FE of the formulated MSA bath was near 100%.

3.2 Tribological Behavior

Considering the results of electrodeposition experiments, two coatings were selected to evaluate their tribological and mechanical properties: a deposit obtained from the MSA + D6 + PEG 600 solution at 1 A/dm^2 (Sn-MSA) and one obtained from the commercial PSA bath at 2.5 A/dm^2 (Sn-PSA).

In Table 4, an overview of tin deposit characteristics is presented. These results show that there were no significant differences in micro hardness and roughness between these two coatings. However, the CoF versus time curves (Fig. 7) show that they have a different tribological behavior. The response of Sn-MSA coating at a 5 N load showed an initial CoF value of 0.2, and after 2 min a friction transition from moderate to severe wear appeared, leading to a very high CoF value of ~ 0.85 toward the end of the test. This abrupt variation of CoF

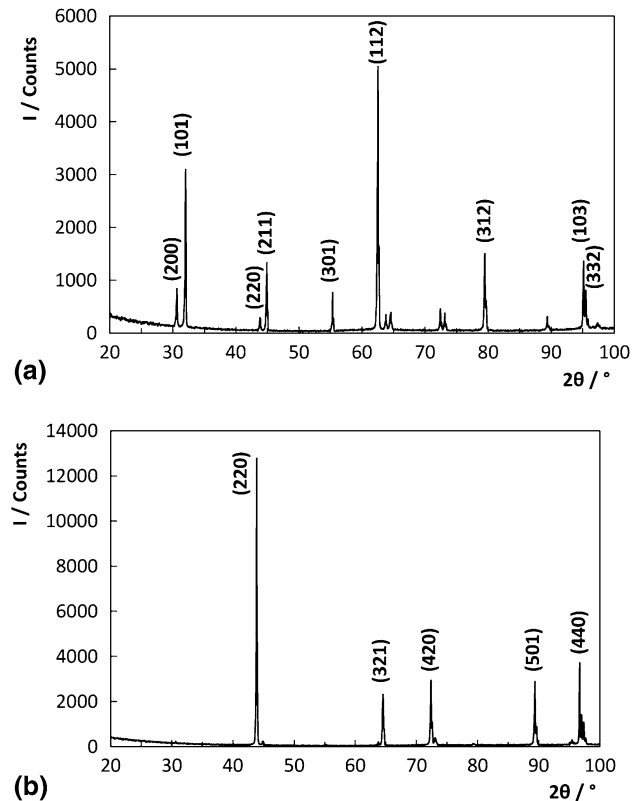


Fig. 6 XRD patterns of Sn deposits obtained from (a) MSA + D6 and (b) MSA + D6 + PEG

is typical of galling processes. In contrast, the Sn-PSA sample showed a low CoF value during the whole test. However, when the load was increased to 10 N both deposits exhibited the same behavior, undergoing galling at different times. These results are in accordance with those reported by Guo et al. (Ref 43), who performed the tribological tests using a ball-on-disk tribometer with a 6 mm diameter 100Cr6 steel ball as the counter-body and 5 N of normal load.

Figure 8 shows a high degree of adhesion and material transfer from the Sn coating surface to the steel counter-body. This phenomenon has been observed in both coatings and under both 5 and 10 N loads. Although the same wear mechanism was operative in all cases, more severe damage was evidenced when 10 N was applied. This held true for both Sn-MSA and Sn-PSA coatings. The appearance of brim shapes (Fig. 9), which are assumed to be generated by the deformation of the superficial layer parallel to the sliding direction, is an evidence of delamination wear. In order to take place, this phenomenon generally requires both low stiffness and high toughness of the material under large adhesion forces (Ref 44).

In this case, the coatings are softer than both the steel substrate and the counter-body, thus ploughing develops under both load regimes (Ref 45). In addition to this, contact pressure exceeds the plastic shakedown limit of the material leading to a severe mass loss generated by plastic ratcheting. The latter, as described by Kapoor (Ref 46), is characterized by a progressive compression of the material due to repeated sliding and the following extrusion of that material to the sides. As a result of this process, slivers are formed which, subsequently, break off producing the loss of material. Figure 9 shows the development of large slivers and plastically deformed ridges in the Sn-MSA

Table 4 Overview of roughness, thickness and Vickers micro hardness

Coating	Roughness parameter, μm			Thickness, μm	Microhardness HV _{0.01}
	R_a	R_z	R_t		
Sn-PSA	1.2 ± 0.1	10.2 ± 2.4	14.4 ± 1.3	43 ± 1	12 ± 2
Sn-MSA	2.0 ± 0.1	12.4 ± 0.3	16.6 ± 2.3	41 ± 1	11 ± 1

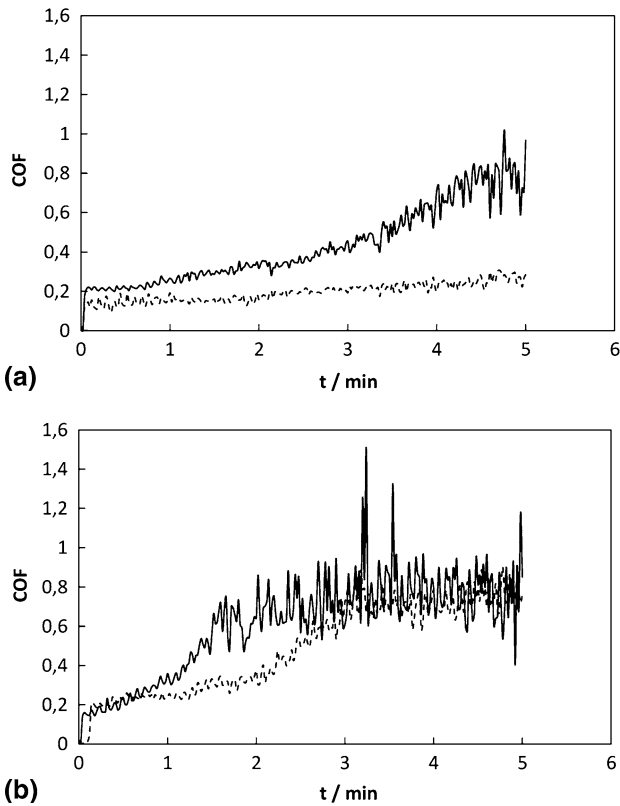


Fig. 7 COF as a function of time at 5 N (dotted line) and 10 N (dashed line) loads. (a) Sn-PSA and (b) Sn-MSA

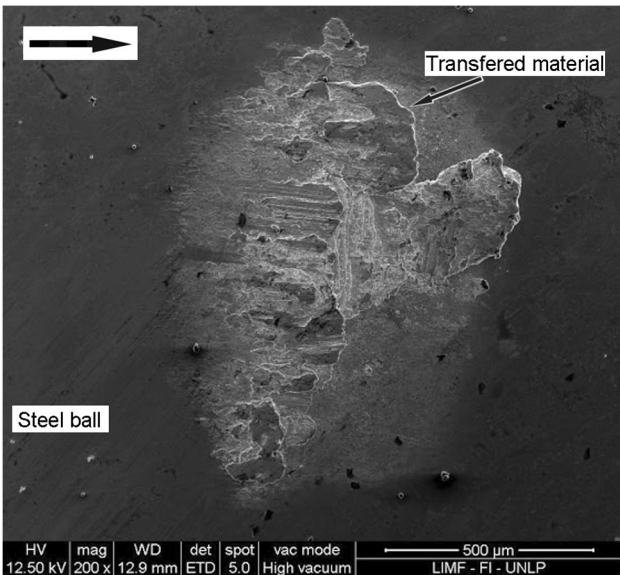


Fig. 8 SEM image at $\times 200$ of steel ball used for testing Sn-PSA coating at 10 N load

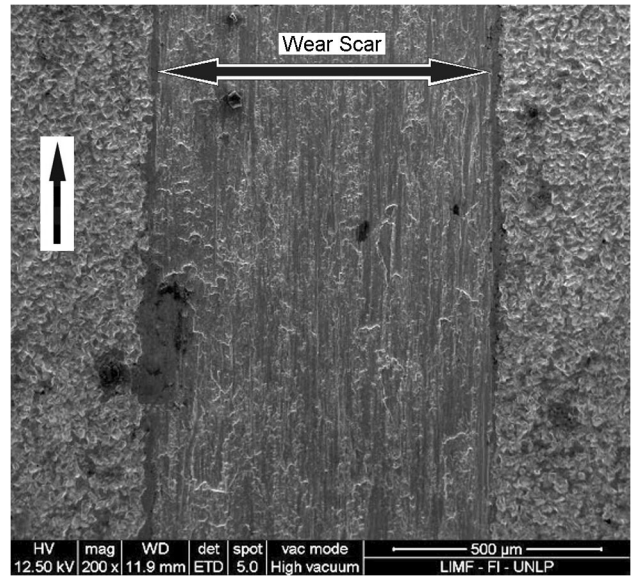


Fig. 9 SEM image at $\times 200$ of Sn-MSA coating's wear track tested at 5 N load

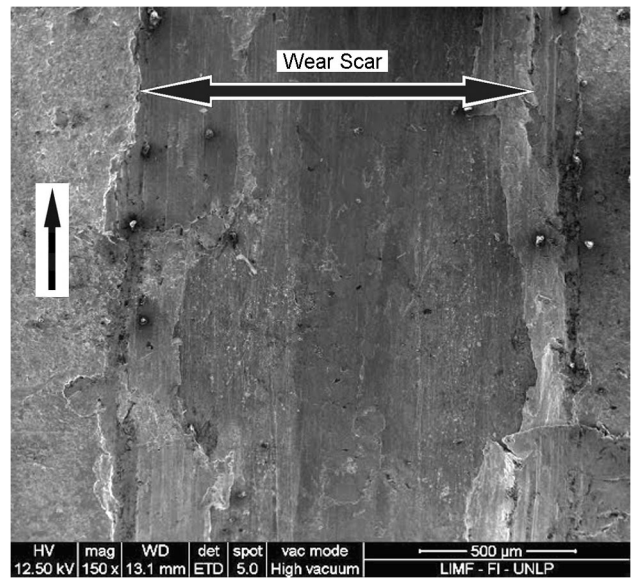


Fig. 10 SEM image at $\times 150$ of Sn-PSA coating's wear track tested at 10 N load

coating tested at 5 N, evidencing severe adhesion between the surfaces. A similar surface morphology had developed at 10 N, with a higher damage level. On the other hand, the Sn-PSA coating tested at 10 N (Fig. 10) presented a more uniform worn surface with less pronounced slivers in comparison to the Sn-MSA specimens. Track width and wear volume results obtained

Table 5 Friction coefficients and wear volumes obtained from the tests made at 5 and 10 N

Coating	Applied load, N			
	5		10	
	COF	Wear volume, mm ³	COF	Wear volume, mm ³
Sn-PSA	0.19	4.54	0.20-0.70	6.8 ± 0.8
Sn-MSA	0.22-0.70	8.40	0.22-0.70	11.3 ± 0.5

for each type of coating (Table 5) clearly show that Sn-PSA coatings have a higher wear resistance than Sn-MSA deposits.

4. Conclusions

In this work, the electrodeposition of tin coatings from different baths was studied. Special attention was paid to the modification of the micro and macro properties of the deposits induced by changes in electrolyte chemistry. For that purpose, a MSA-based solution similar to an industrial PSA bath was formulated. Smooth, adherent, and bright tin coatings were produced using the aforementioned electrolyte at high Faradaic efficiencies.

Cyclic voltammetry showed that the addition of D6 to the MSA electrolyte strongly inhibits tin cathodic reaction, which prevents dendrite's growth. In addition, PEG 600 has little effect on the current response of tin deposition, although it induces a further polarization of the cathodic process.

SEM micrographs and XRD measurements showed that tin deposits obtained from MSA electrolyte and tin industrial coatings (produced using a PSA bath) have different morphologies and textures. Moreover, these variations modified the appearance, mainly brightness, of the deposits. In particular, PEG addition to the MSA electrolyte strongly promotes the growth of 440 and 220 planes during build-up of the tin coating. Regarding the tribological performance, both coatings presented similar initial coefficient of friction and underwent galling a few minutes after the beginning of the test. However, the results proved that Sn-PSA deposits have a higher wear resistance. Once again, these differences in macroscopic properties can be ascribed to changes at a microscopic level.

The results presented in this paper demonstrate the importance of evaluating coating performance when the supporting electrolyte is changed. This determines whether the resulting coatings are suitable or not for the same application of industrial deposits and, hence the capability of a bath to replace the ones currently used.

Acknowledgments

The authors would like to thank the Comisión de Investigaciones Científicas de la Provincia de Buenos Aires (CICPBA), Consejo Nacional de Investigaciones Científicas y Técnicas (CONICET), Universidad Nacional de La Plata (UNLP) and Universidad Nacional del Sur (UNS) for the financial support provided. This research was partially financed by SIDERCA S.A.I.C. (Tenaris) through a collaboration agreement with CONICET.

References

1. R. Winand, Electrocrystallization—Theory and Applications, *Hydrometallurgy*, 1992, **29**, p 567–598
2. M.E. Browning, *Plating and Electroplating*, Surface Engineering. ASM International, New York, 1994, p 239–242
3. M. Schlesinger and M. Paunovic, *Modern Electroplating*, 5th ed., Wiley, New Jersey, 2010
4. T.P. Murphy and H. Smith, Changes in Tinplate Surfaces During DWI Can Manufacture, in *3rd International Tinplate Conference, Conference Date (London)*, 1984, p 299–309
5. D. Thomson, D.A. Luke, and C. Mosher, Reducing Tin Sludge in Acid Tin Plating, 1995, US 5,378,347
6. A. Survila, Z. Mockus, and R. Juškėnas, Current Oscillations Observed During Codeposition of Copper and Tin from Sulfate Solutions Containing Laprol 2402C, *Electrochim. Acta*, 1998, **43**(8), p 909–917
7. G.I. Medvedev, N.A. Makrushin, and O.V. Ivanova, Electrodeposition of Copper-Tin Alloy from Sulfate Electrolyte, *Russ. J. Appl. Chem.*, 2004, **77**(7), p 1104–1107
8. E. Ilgar, Electrolytic Tin Plating Process with Reduced Sludge Production, 1998, US 5,814,202
9. E. Morgan, *Tinplate Manufacture, Tinplate & Modern Canmaking Technology (Chap. 2)*, E. Morgan, Ed., Pergamon, Oxford, 1985, p 5–73
10. A. Sharma, S. Bhattacharya, R. Sen, B.S.B. Reddy, H.J. Fecht, K. Das, and S. Das, Influence of Current Density on Microstructure of Pulse Electrodeposited Tin Coatings, *Mater. Charact.*, 2012, **68**, p 22–32
11. U. Sahaym, S.L. Miller, and M.G. Norton, Effect of Plating Temperature on Sn Surface Morphology, *Mater. Lett.*, 2010, **64**(14), p 1547–1550
12. G.-S. Tzeng, Effects of Additive Agents on the Kinetics of Tin Electrodeposition from an Acidic Solution of Tin(II) Sulfate, *Plat. Surf. Finish.*, 1995, **82**, p 67–71
13. F. Bottos, B. Alavanjo, M. Steel, G. Federman, and J. Swanson, Commercial Production of Tinplate with an MSA Process on a Horizontal Cell Tinplate Line at National Steel's Midwest Division, *6th International Tinplate Conference, Conference Date (London)*, 1996, p 38–59
14. G. Federman, An Improved High Speed MSA Tinplate Process: Laboratory Testing to Production Experience, *7th International Tinplate Conference, Conference Date (Amsterdam)*, 2000
15. C. Rosenstein, Methane Sulfonic Acid as an Electrolyte for Tin, Lead and Tin-Lead Plating for Electronics, *Metal Finish.*, 1990, **88**, p 17–21
16. Y.-H. Yau, The Effect of Process Variables on Electrotinning in a Methanesulfonic Acid Bath, *J. Electrochem. Soc.*, 2000, **147**(3), p 1071–1076
17. N.M. Martyak and R. Seefeldt, Additive-Effects During Plating in Acid Tin Methanesulfonate Electrolytes, *Electrochim. Acta*, 2004, **49**, p 4303–4311
18. C.T.J. Low and F.C. Walsh, The Influence of a Perfluorinated Cationic Surfactant on the Electrodeposition of Tin from a Methanesulfonic Acid Bath, *J. Electroanal. Chem.*, 2008, **615**, p 91–102
19. W. Zhang, J. Guebey, and M. Toben, A novel Electrolyte for the high Speed Electrodeposition of Bright Pure Tin at Elevated Temperatures, *Metal Finish.*, 2011, **109**(1-2), p 13–19
20. F.I. Nobel, B.D. Ostrow, and D.N. Schram, Tin-Lead Electroplating Solutions, 1988, US 4,717,460
21. F.I. Nobel, B.D. Ostrow, and D.N. Schram, Bath and Process for Plating Tin, Lead and Tin-Lead Alloys, 1986, US 4,565,609
22. K. Obata, N. Dohi, Y. Okuhama, S. Masaki, Y. Okada, and M. Yoshimoto, Tin, Lead, and Tin-Lead Alloy Plating Baths, 1984, US 4,459,185

23. C. Xu, Y. Zhang, C. Fan, P. Chiu, and J.A. Abys, Surface morphology, appearance and tribology of electrodeposited tin films, *Plat. Surf. Finish.*, 2000, **87**(9), p 88–92
24. C. Xu, Y. Zhang, P. Chiu, and J.A. Abys, Glossiness, Morphology and Microstructure of Electrodeposited Sn Films, *Surface Finishing*, Conference Date, 1999
25. C.H. O'driscoll, Tin Plating Electrolyte Compositions, 2001, European Patent EP0857226 B1
26. C.T.J. Low, F.C. Walsh, and C. Ponce de Leon, The Rotating Cylinder Electrode (RCE) and its Applications to the Electrodeposition of Metals, *Aust. J. Chem.*, 2005, **58**, p 246–262
27. D.R. Gabe, G.D. Wilcox, J. Gonzalez-Garcia, and F.C. Walsh, The Rotating Cylinder Electrode: Its Continued Development and Application, *J. Appl. Electrochem.*, 1998, **28**(8), p 759–780
28. L.N. Bengoa, W.R. Tuckart, N. Zabala, G. Prieto, and W.A. Egli, Bronze Electrodeposition from an Acidic Non-cyanide High Efficiency Electrolyte: Tribological Behavior, *Surf. Coat. Technol.*, 2014, **253**, p 241–248
29. Y.-F. Tu, X.-H. Chao, J.-P. Sang, S.-Y. Huang, and X.-W. Zou, Thin-Layer Electrodeposition of Zn in the Agar Gel Medium, *Phys. A*, 2008, **387**(16-17), p 4007–4014
30. L.P. Bérubé and G. L'Espérance, A Quantitative Method of Determining the Degree of Texture of Zinc Electrodeposits, *J. Electrochem. Soc.*, 1989, **136**(8), p 2314–2315
31. JCPDS-ICDD, Powder Diffraction Files Sn 04-0673, International Center for Diffraction Data, Newtown Square, 1997
32. S. Wen and J.A. Szipun, Nucleation and Growth of Tin on Low Carbon Steel, *Electrochim. Acta*, 2005, **50**(12), p 2393–2399
33. G. Gunawardena, G. Hills, and I. Montenegro, Electrochemical Nucleation: Part V. Electrodeposition of Cadmium Onto Vitreous Carbon and Tin Oxide Electrodes, *J. Electroanal. Chem.*, 1985, **184**(2), p 371–389
34. M. Moharana and A. Mallik, Nickel Electrocrystallization in Different Electrolytes: An In-Process and Post Synthesis Analysis, *Electrochim. Acta*, 2013, **98**, p 1–10
35. J. Torrent-Burgués, E. Guaus, and F. Sanz, Initial Stages of Tin Electrodeposition from Sulfate Baths in the Presence of Gluconate, *J. Appl. Electrochem.*, 2002, **32**(2), p 225–230
36. E. Gómez, E. Guaus, F. Sanz, and E. Vallés, Tin Electrodeposition on Carbon Electrodes. From Nuclei to Microcrystallites, *J. Electroanal. Chem.*, 1999, **465**(1), p 63–71
37. K.I. Popov, N.V. Krstajić, and M.I. Čekerevac, The Mechanism of Formation of Coarse and Disperse Electrodeposits, *Modern Aspects of Electrochemistry*, R.E. White, B.E. Conway, and J.O.M. Bockris, Ed., Plenum, New York, 1996, p 261–312
38. K.I. Popov and N.D. Nikolic, General Theory of Disperse Metal Electrodeposits Formation, *Electrochemical Production of Metal Powders*, S.S. Djokić, Ed., Springer, New York, 2012, p 1–62
39. G.I. Medvedev, N.A. Makrushin, and A.N. Dubenkov, Organic Compounds for Preparing Lustrous Tin Coatings, *Russ. J. Appl. Chem.*, 2002, **75**(11), p 1799–1803
40. G.I. Medvedev and N.A. Makrushin, A Study of the Kinetics of Tin Electrodeposition from Sulfate Electrolyte with Organic Additives, *Russ. J. Appl. Chem.*, 2002, **75**(8), p 1234–1236
41. F.J. Barry and V.J. Cunnane, Synergistic Effects of Organic Additives on the Discharge, Nucleation and Growth Mechanisms of Tin at Polycrystalline Copper Electrodes, *J. Electroanal. Chem.*, 2002, **537**, p 151–163
42. R. Sekar, C. Eagammai, and S. Jayakrishnan, Effect of Additives on Electrodeposition of Tin and Its Structural and Corrosion Behaviour, *J. Appl. Electrochem.*, 2010, **40**(1), p 49–57
43. X. Guo, G. Zhang, W. Li, Y. Gao, H. Liao, and C. Coddet, Investigation of the Microstructure and Tribological Behavior of Cold-Sprayed Tin-Bronze-Based Composite Coatings, *Appl. Surf. Sci.*, 2009, **255**(6), p 3822–3828
44. X. Guo, G. Zhang, W. Li, L. Dembiski, Y. Gao, H. Liao, and C. Coddet, Microstructure, Microhardness and Dry Friction Behavior of Cold-Sprayed Tin Bronze Coatings, *Appl. Surf. Sci.*, 2007, **254**(5), p 1482–1488
45. K. Holmberg, A. Matthews, and H. Ronkainen, Coatings Tribology—Contact Mechanisms and Surface Design, *Tribol. Int.*, 1998, **31**(1-3), p 107–120
46. A. Kapoor, Wear by Plastic Ratchetting, *Wear*, 1997, **212**, p 119–130